Journal of
Applied Remote Sensing

RemoteSensing.SPIEDigitalLibrary.org

Updates of Moderate Resolution Imaging Spectroradiometer on-orbit calibration uncertainty assessments

Xiaoxiong Xiong
Amit Angal
William L. Barnes
Hongda Chen
Vincent Chiang
Xu Geng
Yonghong Li
Kevin Twedt
Zhipeng Wang
Truman Wilson
Aisheng Wu

SPIE.

Xiaoxiong Xiong, Amit Angal, William L. Barnes, Hongda Chen, Vincent Chiang, Xu Geng, Yonghong Li, Kevin Twedt, Zhipeng Wang, Truman Wilson, Aisheng Wu, "Updates of Moderate Resolution Imaging Spectroradiometer on-orbit calibration uncertainty assessments," *J. Appl. Remote Sens.* **12**(3), 034001 (2018), doi: 10.1117/1.JRS.12.034001.

Updates of Moderate Resolution Imaging Spectroradiometer on-orbit calibration uncertainty assessments

Xiaoxiong Xiong,[a,*] Amit Angal,[b] William L. Barnes,[c] Hongda Chen,[b] Vincent Chiang,[b] Xu Geng,[b] Yonghong Li,[b] Kevin Twedt,[b] Zhipeng Wang,[b] Truman Wilson,[b] and Aisheng Wu[b]

[a]NASA GSFC, Sciences and Exploration Directorate, Greenbelt, Maryland, United States
[b]Science Systems and Applications Inc., Lanham, Maryland, United States
[c]University of Maryland, Baltimore County, Baltimore, Maryland, United States

Abstract. The Moderate Resolution Imaging Spectroradiometer (MODIS) instruments have successfully operated for more than 18 and 16 years, respectively, on-board the NASA's Earth Observing System Terra and Aqua spacecraft. Both Terra and Aqua MODIS have significantly contributed to the advance of global Earth remote sensing applications with a broad range of science products that have been continuously produced since the beginning of each mission and freely distributed to users worldwide. MODIS collects data in 20 reflective solar bands (RSB) and 16 thermal emissive bands (TEB), covering wavelengths from 0.41 to 14.4 μm. Its level 1B (L1B) data products, which provide the input for the MODIS high-level science products, include the top of the atmosphere reflectance factors for the RSB, radiances for both the RSB and TEB, and associated uncertainty indices (UI) at a pixel-by-pixel level. This paper provides a brief review of MODIS L1B calibration algorithms, including a number of improvements made in recent years. It presents an update of sensor calibration uncertainty assessments with a focus on several new contributors resulting from on-orbit changes in sensor characteristics, approaches developed to address these changes, and the impact due to on-orbit changes on the L1B data quality. Also discussed are remaining challenges and potential improvements to be made to continuously maintain sensor calibration and data quality, particularly those related to the quality of MODIS L1B uncertainty. [DOI: 10.1117/1.JRS.12.034001]

Keywords: moderate resolution imaging spectroradiometer; terra; aqua; calibration; characterization; traceability; uncertainty.

Paper 180356 received Apr. 27, 2018; accepted for publication Jun. 26, 2018; published online Jul. 16, 2018.

1 Introduction

The Moderate Resolution Imaging Spectroradiometer (MODIS) is one of the key instruments for the NASA Earth Observing System (EOS) Terra and Aqua missions that have operated successfully for more than 18 and 16 years since their launches in December 1999 and May 2002, respectively.[1–4] MODIS is a scanning radiometer that collects data in 36 spectral bands, covering wavelengths from visible to long-wave infrared, and at three spatial resolutions (nadir): 250 m (bands 1 to 2), 500 m (bands 3 to 7), and 1 km (bands 8 to 36). It was developed and designed with significant advancements over its heritage sensors, such as the advanced very high resolution radiometer (AVHRR) and the Landsat Thematic Mapper (TM). Methodologies and strategies developed and lessons learned from MODIS design, prelaunch testing, and on-orbit operation and calibration have greatly benefited the development of many follow-on

*Address all correspondence to: Xiaoxiong Xiong, E-mail: xiaoxiong.xiong-1@nasa.gov

1931-3195/2018/$25.00 © 2018 SPIE

Earth-observing sensors, including the S-NPP and Joint Polar Satellite System visible infrared imaging radiometer suite (VIIRS) instruments and the Landsat-8 operational land imager.[5–8]

Over the course of their entire missions, both Terra and Aqua MODIS instruments have generated an unprecedented amount of data products that are openly distributed to the science community and users worldwide, enabling and supporting a broad range of studies of the Earth's system that include the short- and long-term changes in its key environmental parameters.[9,10] The quality and calibration uncertainty of MODIS level 1B (L1B) data products are extremely important as they provide key input for generating the high-level science products. The MODIS L1B data products include top of the atmosphere reflectance factors for the reflective solar bands (RSB), radiances for both the RSB and thermal emissive bands (TEB), and the associated uncertainty indices (UI) on a pixel-by-pixel level.[11–13]

MODIS 36 spectral bands, consisting of a total of 490 individual detectors, are distributed on four focal plane assemblies (FPAs) according to their wavelengths, as shown in Fig. 1: visible (VIS), near-infrared (NIR), short- and midwave infrared (SWIR/MWIR or SMIR), and longwave infrared (LWIR). The SMIR and LWIR FPAs are nominally controlled at 83 K, thus referred to as the cold FPAs. Bands 1 to 19 and 26 are the RSB, covering wavelengths from 0.41 to 2.3 μm, and bands 20 to 25 and 27 to 36 are the TEB, covering wavelengths from 3.75 to 14.4 μm. Table 1 is a summary of key design parameters of MODIS spectral bands, including their bandwidths, typical spectral radiances, required signal-to-noise ratios (SNRs) or noise equivalent temperature differences at typical radiances, and their primary applications. In addition to extensive prelaunch testing and measurements made to assess instrument performance, MODIS spectral bands are regularly calibrated and characterized on-orbit by a set of on-board calibrators (OBCs). As shown in Fig. 2, MODIS OBCs include a solar diffuser (SD), a solar diffuser stability monitor (SDSM), a blackbody (BB), a spectroradiometric calibration assembly, and a space view (SV) port.

MODIS radiometric calibration uncertainty requirements are 2% in reflectance and 5% in radiance for the RSB and 1% in radiance for the TEB, with exceptions of 0.5% for surface temperature spectral bands 31 and 32 at 11 and 12 μm, 0.75% for band 20 at 3.75 μm, and 10% for band 21 (used for fire detection) at 3.95 μm. These requirements are specified at typical scene radiance levels of individual spectral bands and for the observations made at scan angles within ± 45 deg. At other radiances between 0.3 typical radiance (0.3 L_{typ}) and 0.9 maximum radiance (0.9 L_{max}), an additional 1% uncertainty is added to those specified at the typical radiance levels.[14]

MODIS RSB and TEB calibration uncertainty algorithms were reported previously in a number of Refs. 15–17. Since then a number of updates have been made due to changes in

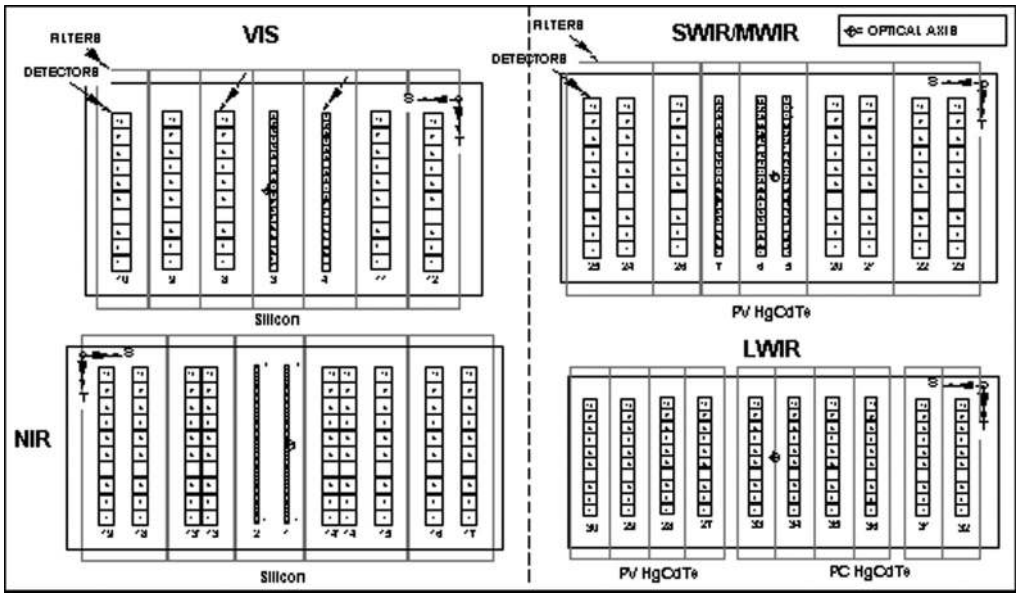

Fig. 1 MODIS FPAs: VIS, NIR, SWIR/MWIR, and LWIR.

Table 1 Key design parameters of MODIS spectral bands.

Primary Use	Band[a]	Bandwidth (nm)	Spectral radiance[b]	Required SNR	Primary use	Band[a]	Bandwidth (nm)	Spectral radiance[b]	Required NEΔT (K)
Land/cloud/aerosols boundaries	1	620 to 670	21.8	128	Surface/cloud temperature	20	3.660 to 3.840	0.45 (300K)	0.05
	2	841 to 876	24.7	201		21	3.929 to 3.989	2.38 (335K)	0.2
Land/cloud/aerosols properties	3	459 to 479	35.3	243		22	3.929 to 3.989	0.67 (300K)	0.07
	4	545 to 565	29	228		23	4.020 to 4.080	0.79 (300K)	0.07
	5	1230 to 1250	5.4	74	Atmospheric temperature	24	4.433 to 4.498	0.17 (250K)	0.25
	6	1628 to 1652	7.3	275		25	4.482 to 4.549	0.59 (275K)	0.25
	7	2105 to 2155	1	110	Cirrus clouds water vapor	26	1.360 to 1.390	6	150 (SNR)
Ocean color/ phytoplankton/ biogeochemistry	8	405 to 420	44.9	880		27	6.535 to 6.895	1.16 (240K)	0.25
	9	438 to 448	41.9	838		28	7.175 to 7.475	2.18 (250K)	0.25
	10	483 to 493	32.1	802	Cloud properties	29	8.400 to 8.700	9.58 (300K)	0.05
	11	526 to 536	27.9	754	Ozone	30	9.580 to 9.880	3.69 (250K)	0.25
	12	546 to 556	21	750	Surface/cloud temperature	31	10.780 to 11.280	9.55 (300K)	0.05
	13	662 to 672	9.5	910		32	11.770 to 12.270	8.94 (300K)	0.05
	14	673 to 683	8.7	1087	Cloud top altitude	33	13.185 to 13.485	4.52 (260K)	0.25
	15	743 to 753	10.2	586		34	13.485 to 13.785	3.76 (250K)	0.25
	16	862 to 877	6.2	516		35	13.785 to 14.085	3.11 (240K)	0.25
Atmospheric water vapor	17	890 to 920	10	167		36	14.085 to 14.385	2.08 (220K)	0.35
	18	931 to 941	3.6	57					
	19	915 to 965	15	250					

[a]Spatial resolution: 250 m (B1 to 2), 500 m (B3 to 7), 1000 m (B8 to 36).
[b]Spectral radiance unit: W/m^2 μm sr.

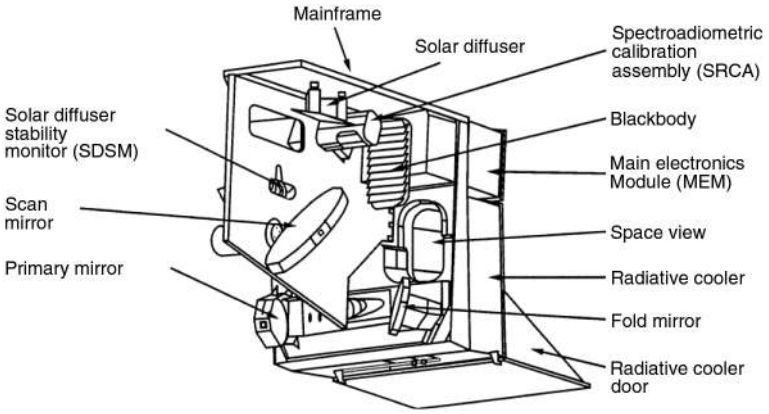

Fig. 2 MODIS instrument scan cavity showing the location of key OBC and optical components.

sensor on-orbit performance and improvements of calibration algorithms. As expected, the calibration uncertainty is scene dependent. It is described in MODIS L1B by an uncertainty index (UI) at a pixel-by-pixel level. The UI in the L1B uncertainty product holds eight-bit unsigned integers. The four least significant bits of these integers are currently effective, with UI values ranging from 0 to 15. The other four bits are reserved for future use. Each UI value represents an interval of uncertainty values that cover the estimated uncertainty. A log scaling is used to convert the calculated uncertainty to UI in the L1B processing to allow a broad range of uncertainty to be covered while an adequate resolution for small uncertainties is still retained. To convert the UI back to the percentage uncertainty, the required parameters are provided for L1B users in the attributes associated with each UI dataset.[11,12]

Before collection 6, the UI had only a few time-dependent terms and most contributors were determined from prelaunch measurements or estimates. Starting from C6, RSB response versus scan-angle (RVS) characterization has included the use of pseudoinvariant ground targets to track changes in sensor responses at multiple angles of incidence (AOIs). Application of a detector-dependent RVS is also made to several VIS spectral bands. These, coupled with other changes made in C6, led to modifications of MODIS L1B uncertainty estimates and therefore the L1B uncertainty product. Similar to RSB calibration coefficients, several time-dependent look-up tables (LUTs) are now provided as the input for generating the L1B uncertainty product.

This paper provides an overview of MODIS on-orbit calibration and uncertainty algorithms and the latest updates resulting from changes in sensor characteristics, such as RVS for the RSB and electronic crosstalk for the long-wave TEB. It serves as an update to our previous references on MODIS calibration uncertainties, including key contributors to the current L1B uncertainty product and strategies developed to implement the changes in the L1B algorithm for its uncertainty estimation. Remaining challenges and future improvements that have impact on the quality of MODIS L1B uncertainty product are also discussed in this paper. Like its calibration algorithms, the MODIS L1B calibration uncertainty approach has also been applied to other Earth-observing sensors, including its follow-on VIIRS instruments.[18,19]

2 Calibration Algorithms

MODIS RSB on-orbit calibration is reflectance based using an on-board SD panel with its bidirectional reflectance factor (BRF) determined prelaunch by the instrument vendor with traceability to the NIST reflectance standard.[20] For a given Earth view (EV) pixel, the calibration is performed for each band, detector, subsample, and mirror side. The MODIS L1B primary deliverable product for the RSB is the EV reflectance factor that can be expressed as

$$\rho_{\mathrm{EV}} \cos(\theta_{\mathrm{EV}}) = m_1 dn^*_{\mathrm{EV}} d^2_{\mathrm{ES\_EV}} / \mathrm{RVS}_{\mathrm{EV}}, \tag{1}$$

where ρ_{EV} is the EV scene BRF, θ_{EV} is the EV solar illumination angle, $dn^*{}_{\mathrm{EV}}$ is the EV digital response corrected for background and instrument temperature, $d_{\mathrm{ES\_EV}}$ is the Earth–Sun distance at the time of the EV measurement in astronomical units (AU), $\mathrm{RVS}_{\mathrm{EV}}$ is the RVS angle at the

EV AOI, and m_1 is the calibration coefficient for the reflectance factor that is determined from SD calibration

$$m_1 = \frac{\rho_{\mathrm{SD}} \cos(\theta_{\mathrm{SD}})}{dn^*_{\mathrm{SD}} \cdot d^2_{\mathrm{ES\_SD}}} \cdot \Gamma_{\mathrm{SDS}} \cdot \Delta_{\mathrm{SD}}, \tag{2}$$

where ρ_{SD} is the SD BRF determined from prelaunch measurements, θ_{SD} is the SD solar illumination angle, $dn^*{}_{\mathrm{SD}}$ is the SD digital response corrected for background and instrumental temperature, $d_{\mathrm{ES\_SD}}$ is the Earth–Sun distance at the time of the SD measurement in AU, Δ_{SD} is SD BRF on-orbit degradation determined by the SDSM, and Γ_{SDS} is the SDS vignetting function used for calibration of the high gain bands (B8-16). Specifically, the corrected digital responses in Eqs. (1) and (2) can be expressed as

$$dn^*_{\mathrm{EV}} = dn_{\mathrm{EV}}[1 + k_{\mathrm{INST}}(T_{\mathrm{INST\_EV}} - T_{\mathrm{INST\_REF}})] \tag{3}$$

and

$$dn^*_{\mathrm{SD}} = dn_{\mathrm{SD}}[1 + k_{\mathrm{INST}}(T_{\mathrm{INST\_SD}} - T_{\mathrm{INST\_REF}})], \tag{4}$$

where dn_{EV} and dn_{SD} are the EV and SD view responses with the background SV response (averaged over the frames within a scan) subtracted, k_{INST} is an instrument temperature correction coefficient determined prelaunch, $T_{\mathrm{INST\_EV}}$ and $T_{\mathrm{INST\_SD}}$ are the instrument temperatures at the time of EV and SD observations, and $T_{\mathrm{INST\_REF}}$ is the reference temperature. The calibration coefficients are determined off-line and updated as necessary to the L1B calibration algorithms via LUTs.

The RVS is normalized at the AOI of the SD—the primary calibration target for the RSB. For other AOIs, the RVS was measured prelaunch and is updated on orbit. The RVS on-orbit variation at the AOI of the SV is tracked by comparing the results of near-monthly lunar calibration events to the results from the SD calibration events. In practice, the inverse of the corrected digital signal from the moon is calculated for each lunar calibration event and then normalized to the mission start value to determine the on-orbit change, $m_1^{\mathrm{moon,oo}}$. This is divided from the on-orbit change in the SD, m_1^{oo}, to get the on-orbit change in the RVS

$$\mathrm{RVS}_{\mathrm{SV}} = \mathrm{RVS}_{\mathrm{SV,prl}} \frac{m_1^{\mathrm{oo}}}{m_1^{\mathrm{moon,oo}}}, \tag{5}$$

where $\mathrm{RVS}_{\mathrm{SV,prl}}$ is the prelaunch RVS at the SV AOI.

For most RSB, the RVS on-orbit variation at other AOI is derived using the SD and lunar data and assumes a linear AOI dependence. This approach works well at the mission beginning and for spectral bands with small on-orbit changes in their responses. However, after many years of on-orbit operations, there was sufficient evidence to suggest that the linear approximation used to track the on-orbit variation in the RVS might be inadequate, especially for the VIS bands that have experienced large on-orbit changes in their responses. In addition, the SD has experienced significant degradation in the VIS wavelengths that might lead to an inaccurate estimation of the gain at the SD AOI. However, the moon, being an extremely stable calibration target, is still considered a reliable source for tracking the gain at the SV AOI and nearby scan angles. To overcome the limitations mentioned above, a new RVS approach, that includes the use of pseudoinvariant EV targets, was developed and implemented starting from C6.[13] This approach uses lunar measurements and response trending from pseudoinvariant desert targets at multiple AOIs. The combination of m_1 and RVS derived using this approach is currently applied in both C6 and C6.1 for Terra bands 1 to 4 and 8 to 10 and Aqua bands 1 to 4, 8, and 9, respectively. In this case, we can write

$$\frac{m_1}{\mathrm{RVS}_{\mathrm{EV}}} = \left(\frac{m_1(t_0)}{\mathrm{RVS}_{\mathrm{EV,prelaunch}}}\right)\left(\frac{m_1}{\mathrm{RVS}_{\mathrm{EV}}}\right)_{\mathrm{on\text{-}orbit}}, \tag{6}$$

where $\left(\frac{m_1}{\mathrm{RVS}_{\mathrm{EV}}}\right)_{\mathrm{on\text{-}orbit}}$ is normalized to 1 at the time when the instrument nadir door was first opened.

MODIS TEB are calibrated on-orbit using an on-board BB. The calibration is performed on a scan-by-scan basis via a quadratic algorithm. The MODIS L1B deliverable product for the TEB is the EV radiance L_{EV} given by the following equation:

$$\mathrm{RVS_{EV}} \cdot L_{\mathrm{EV}} + (\mathrm{RVS_{SV}} - \mathrm{RVS_{EV}}) \cdot L_{\mathrm{SM}} = a_0 + b_1 \cdot dn_{\mathrm{EV}} + a_2 \cdot dn_{\mathrm{EV}}^2, \tag{7}$$

where L_{SM} is the radiance due to scan mirror (SM) emission, $\mathrm{RVS_{EV}}$ and $\mathrm{RVS_{SV}}$ are the system RVS angles at the EV and SV. The EV digital response $\mathrm{dn_{EV}}$ is corrected for the instrument background using the sensor's SV response. The offset and quadratic calibration coefficients (a_0 and a_2) are determined from BB warm-up and cool-down, whereas the linear coefficient (b_1) is computed each scan using the sensor's response to the BB

$$\begin{aligned}\mathrm{RVS_{BB}} \cdot \varepsilon_{\mathrm{BB}} \cdot L_{\mathrm{BB}} + (\mathrm{RVS_{SV}} - \mathrm{RVS_{BB}}) \cdot L_{\mathrm{SM}} + \mathrm{RVS_{BB}} \\ \cdot (1 - \varepsilon_{\mathrm{BB}}) \cdot \varepsilon_{\mathrm{CAV}} \cdot L_{\mathrm{CAV}} = a_0 + b_1 \cdot dn_{\mathrm{BB}} + a_2 \cdot dn_{\mathrm{BB}}^2,\end{aligned} \tag{8}$$

where L_{BB} and L_{CAV} are the BB and scan cavity (CAV) radiances and $\varepsilon_{\mathrm{BB}}$ and $\varepsilon_{\mathrm{CAV}}$ are their emissivities. $\mathrm{RVS_{BB}}$ is the system RVS at the BB view. The sensor's response to BB, dn_{BB}, is also corrected for the instrument background. Equations (7) and (8) are nearly identical except a cavity term included in the BB calibration equation. This is due to the scan cavity emission (L_{CAV}) reflected from the BB surface with an equivalent reflectivity of $1 - \varepsilon_{\mathrm{BB}}$. In MODIS TEB calibration, the entire RVS curve is normalized to the BB view at an angle of incidence of 26.5 deg. The calibration is band, detector, and mirror side dependent. The radiance terms in the calibration equations (L_{BB}, L_{SM}, and L_{CAV}) are computed using Planck's equation weighted over each detector's relative spectral response at their corresponding temperatures. The BB, SM, and instrument cavity temperatures are provided in the instrument telemetry records.

Details of Terra and Aqua MODIS RSB and TEB calibration algorithms can be found in a number of Refs. 21–24. In addition to the baseline algorithms described above, MODIS RSB calibration has included a correction to mitigate the impact due to a thermal leak and electronic crosstalk in the SWIR bands 5 to 7 and 26.[25] For the TEB, an optical leak correction is applied for Terra MODIS photoconductive (PC) bands 32 to 36 from the beginning of its mission,[22] and, recently, an electronic crosstalk correction is also applied to its photovoltaic (PV) bands 27to 30.[26] Band 21 is used for fire detection with a low gain setting, and its on-orbit calibration is performed with fixed linear gain provided in the calibration LUTs.

3 Reflective Solar Bands Calibration Uncertainty

Combining Eqs. (1)–(4), the EV reflectance factor at the SD AOI can be written as

$$[\rho_{\mathrm{EV}} \cos(\theta_{\mathrm{EV}})]_{\mathrm{SD}} = \rho_{\mathrm{SD}} \cos(\theta_{\mathrm{SD}}) \Gamma_{\mathrm{SDS}} \Delta_{\mathrm{SD}} \frac{dn_{\mathrm{EV}} d_{\mathrm{ES,EV}}^2 [1 + k_{\mathrm{inst}}(T_{\mathrm{INST\_EV}} - T_{\mathrm{INST\_REF}})] \mathrm{RVS_{SD}}}{dn_{\mathrm{SD}} d_{\mathrm{ES,SD}}^2 [1 + k_{\mathrm{inst}}(T_{\mathrm{INST\_SD}} - T_{\mathrm{INST\_REF}})] \mathrm{RVS_{EV}}}. \tag{9}$$

Therefore, the total uncertainty of the reflectance factor at the SD AOI can be written as the root mean square (RMS) summation of the uncertainty associated with the parameters on the right-hand side of Eq. (9)

$$\begin{aligned}\left[\frac{\delta\rho_{\mathrm{EV}} \cos(\theta_{\mathrm{EV}})}{\rho_{\mathrm{EV}} \cos(\theta_{\mathrm{EV}})}\right]_{\mathrm{SD}}^2 = \left[\frac{\delta\rho_{\mathrm{SD}}}{\rho_{\mathrm{SD}}}\right]^2 + \left[\frac{\delta\Gamma_{\mathrm{SDS}}}{\Gamma_{\mathrm{SDS}}}\right]^2 + \left[\frac{\delta\Delta_{\mathrm{SD}}}{\Delta_{\mathrm{SD}}}\right]^2 + \left[\frac{\delta dn_{\mathrm{SD}}}{dn_{\mathrm{SD}}}\right]^2 + \left[\frac{\delta dn_{\mathrm{EV}}}{dn_{\mathrm{EV}}}\right]^2 + \left[\frac{\delta \mathrm{RVS_{EV}}}{\mathrm{RVS_{EV}}}\right]^2 + \\ [\delta k_{\mathrm{inst}}(T_{\mathrm{INST\_EV}} - T_{\mathrm{INST\_SD}})]^2 + [k_{\mathrm{inst}} \delta(T_{\mathrm{INST\_EV}} - T_{\mathrm{INST\_SD}})]^2,\end{aligned} \tag{10}$$

where the terms related to Earth–Sun distance and SD solar illumination angle have negligible contributions to the uncertainty and therefore have been dropped. Also ignored in Eq. (8) is the $\mathrm{RVS_{SD}}$ term as RSB RVS is normalized to the SD AOI. The covariance terms are all expected to be small and are not considered here.

The dominant contributor to the RSB calibration uncertainty is related to the SD BRF uncertainty that includes its characterization uncertainty determined from prelaunch measurements and that from on-orbit calibration and characterization. Table 2 shows a summary of uncertainty elements related to SD calibration. The first 6 terms in Table 2 are the uncertainties derived from prelaunch BRF characterization. On-orbit SD uncertainty contributors include items 7 to 9.

Table 2 Summary of MODIS solar diffuser characterization uncertainty elements ($k = 1$).

	Error sources	SBRS	MCST (I)	MCST (II)
1	NIST reference:	0.50	0.50	
2	SBRS scattering goniometer:	0.70	0.70	
3	NIST BRF scale to MODIS SD reference:	0.50	0.50	
4	MODIS SD characterization:	0.50	0.50	
5	SD spatial non-uniformities:	0.70	0.35	
6	Interpolation angular / spectrally:	0.10	0.10	
7	Prelaunch to on-orbit SD BRF change:	0.50	0.50	
8	SD screen (SDS):	0.20		0.50
9	SDSM and SDS impact:	0.50	0.50	
10	Solar illumination of the SD surrounds	0.30		0.50–0.80
11	Earthshine through the SD door	0.30		
12	Earthshine through nadir aperture door	0.10	0.00	
	RSS	1.57	1.37	

Items 10 to 12 are related to the stray light and Earthshine elements that could also impact the on-orbit SD calibration. The second column of Table 2 has listed original uncertainty elements (error sources) reported by the instrument vendor (SBRS). Based on the independent uncertainty analysis performed by the MODIS Characterization Support Team (MCST), we increased the SD screen uncertainty term (item 8) from 0.2% to 0.5%. This adjustment was made due to the fact that no prelaunch characterization was made for the SD screen transmittance (or vignetting function Γ_{SDS}). This term only applies to the bands that are calibrated with the SDS in place. We have also combined the stray light term with the Earthshine term as their contributions are always in the same direction. The magnitude of Earthshine related uncertainty used in the MCST uncertainty analysis is strongly wavelength dependent. As MODIS SD calibration is performed when the instrument is on the dark side of the terminator, we have dropped the term related to the Earthshine through the EV nadir aperture door (0.1%). Based on our on-orbit characterization of SD BRF and how the SD panel is used in RSB calibration, we believe that the SD uniformity impact on the calibration uncertainty is smaller than prelaunch assessment. Additional information on the uncertainty elements listed in Table 2 can be found in these Refs. 27 and 28. Note that the first term on the right-hand side of Eq. (10) includes the combined uncertainty of all elements in the second column of Table 2, in addition to the band-dependent Earthshine uncertainty.

The SD degradation, Δ_{SD}, is determined from SDSM measurements, and the uncertainty in this term is simply taken to be the standard deviation of fitting residuals of the SDSM trends. The last two terms in Eq. (10) represent the uncertainty associated with the prelaunch characterization of the RSB temperature correction coefficients k_{inst} and instrument temperature T_{inst}. These terms are derived using the assumption $k_{\mathrm{inst}}(T_{\mathrm{inst}} - T_{\mathrm{ref}}) \ll 1$. The impact of these two terms is relatively small, each typically $<10^{-3}$. Finally, the terms $\left[\frac{\delta dn_{\mathrm{SD}}}{dn_{\mathrm{SD}}}\right]$ and $\left[\frac{\delta dn_{\mathrm{EV}}}{dn_{\mathrm{EV}}}\right]$ are the uncertainties related to the sensor's SD response noise and EV response noise at typical signal levels. The value of δdn is calculated as a function of dn using a linear approximation to obtain the fitting coefficients ($c_{0,1}$). The data from every SD calibration event are fitted to obtain values for these coefficients for each band, detector, mirror side, and subframe. The noise is then calculated at the typical signal level of the SD calibration to determine the $\left[\frac{\delta dn_{\mathrm{SD}}}{dn_{\mathrm{SD}}}\right]$ term. For the

$\left[\frac{\delta dn_{EV}}{dn_{EV}}\right]$ term, the value depends on the dn_{EV} and is thus evaluated for every EV pixel using the coefficients $c_{0,1}$. This uncertainty term can be significant for very low radiance scenes.[29]

The uncertainty at the SD AOI is determined by considering all of the terms in the SD calibration as just described. This approach has been used in all previous descriptions of MODIS RSB uncertainty. Starting from *C*6, we split m_1/RVS uncertainty terms into those determined prelaunch and those used to capture on-orbit changes. The prelaunch determined uncertainties at the SD AOI represent a baseline uncertainty that is present for all time and AOI, and the uncertainties in the parameters that have on-orbit changes are added to this baseline. For most RSB, the on-orbit m_1 and RVS are derived solely based on the on-board measurements from the SD and moon (viewed via the SV port). Based on Eqs. (1)–(5) and similar to Eq. (10), the total uncertainty of the reflectance factor at the AOI of the SV can be expressed as follows:

$$\left[\frac{\delta\rho_{EV}\cos(\theta_{EV})}{\rho_{EV}\cos(\theta_{EV})}\right]^2_{SV} = \left[\frac{\delta\rho_{SD}}{\rho_{SD}}\right]^2 + \left[\frac{\delta\Gamma_{SDS}(t_0)}{\Gamma_{SDS}(t_0)}\right]^2 + \left[\frac{\delta\Delta_{SD}(t_0)}{\Delta_{SD}(t_0)}\right]^2 + \left[\frac{\delta dn_{SD}(t_0)}{dn_{SD}(t_0)}\right]^2 + \left[\frac{\delta dn_{EV}}{dn_{EV}}\right]^2 + [\delta k_{inst}(T_{inst,EV} - T_{inst,SD})]^2 + [k_{inst}\delta(T_{inst,EV} - T_{inst,SD})]^2 + \left[\frac{\delta RVS_{SV,prl}}{RVS_{SV,prl}}\right]^2 + \left[\frac{\delta m_1^{moon,\,oo}}{m_1^{moon,oo}}\right]^2, \tag{11}$$

where the (t_0) indicates the values of uncertainty at mission start, $\left[\frac{\delta RVS_{SV,prl}}{RVS_{SV,prl}}\right]$ is the prelaunch RVS measurement uncertainty, which is band dependent, and $\left[\frac{\delta m_1^{moon,\,oo}}{m_1^{moon,oo}}\right]$ is the uncertainty in the measurement of the lunar calibration. This lunar uncertainty is calculated from the standard deviation of the fitting residuals after fitting the $m_1^{moon,oo}$ time series to an empirically determined piece-wise function. The other terms in Eq. (11) are the same as in Eq. (10).

At other AOI, the m_1/RVS is determined by assuming a linear dependence of the RVS between the SD and SV (lunar) calibration results. Correspondingly, the uncertainty at arbitrary AOI is a combination of the uncertainties in the on-orbit changes at the SD and SV AOI. For some bands, mirror side ratio data obtained from Earth-view targets are used to supplement the on-board data in calculating the m_1/RVS for mirror side 2. Thus, an additional uncertainty term is also applied to mirror side 2 that accounts for the typical uncertainty in the EV observations. We note that this results in mirror side 2 having a larger uncertainty than mirror side 1 for these bands, which is clearly not appealing as the mirror side labeling is an arbitrary choice. This is an issue that will be addressed in future algorithm changes.

As stated in Sec. 2, on-orbit changes in both the m_1 and RVS for select RSB (Terra bands 1 to 4, 8 to 10, and Aqua bands 1 to 4, 8, and 9) are computed using the lunar measurements and measurements from select EV desert sites.[30,31] In this EV-based approach, the EV reflectance factor can be expressed as follows:

$$[\rho_{EV}\ \cos(\theta_{EV})]_\alpha = \frac{dn_{EV}d^2_{ES,EV}\ [1 + k_{inst}(T_{inst,EV} - T_{inst,ref})]m_1(t_0)}{RVS_{prl}}\left(\frac{m_1}{RVS}\right)_{EV,on\text{-}orbit}, \tag{12}$$

where the α subscript indicates arbitrary AOI. The total uncertainty of the reflectance factor is

$$\left[\frac{\delta\rho_{EV}\cos(\theta_{EV})}{\rho_{EV}\cos(\theta_{EV})}\right]^2_{\alpha} = \left[\frac{\delta\rho_{SD}}{\rho_{SD}}\right]^2 + \left[\frac{\delta\Gamma_{SDS}(t_0)}{\Gamma_{SDS}(t_0)}\right]^2 + \left[\frac{\delta\Delta_{SD}(t_0)}{\Delta_{SD}(t_0)}\right]^2 + \left[\frac{\delta dn_{SD}(t_0)}{dn_{SD}(t_0)}\right]^2 + \left[\frac{\delta dn_{EV}}{dn_{EV}}\right]^2 + [\delta k_{inst}(T_{inst,EV} - T_{inst,SD})]^2 + [k_{inst}\delta(T_{inst,EV} - T_{inst,SD})]^2 + \left[\frac{\delta RVS_{prl}}{RVS_{prl}}\right]^2 + \left[\frac{\delta\left(\frac{m_1}{RVS}\right)_{EV,on\text{-}orbit}}{\left(\frac{m_1}{RVS}\right)_{EV,on\text{-}orbit}}\right]^2. \tag{13}$$

All of the terms in this equation have been previously discussed, except for the last one. The uncertainty in the EV-based m_1/RVS for all AOI is determined from two sets of fitting residuals. First, the normalized reflectance trends from the desert sites are fit to a piecewise polynomial

function of time at several select AOI. Then, the results of the time fitting are fit to a quadratic or quartic function over AOI, depending on the band. The uncertainty due to on-orbit change in the EV m_1/RVS is taken to be the summation of the standard deviation of the fitting residuals of these two fits.

The various components contributing to the MODIS RSB uncertainty algorithm are organized in five different terms (U_1, U_2, U_3, U_4, and U_5) when computing the uncertainty of RSB L1B product. The organization is based on each term's dependence of band (B), detector (D), mirror side (M), subframe (SF), time (t), AOI (θ), and scene

$$\left[\frac{\delta\rho_{\mathrm{EV}}\cos(\theta_{\mathrm{EV}})}{\rho_{\mathrm{EV}}\cos(\theta_{\mathrm{EV}})}\right]_{\alpha}^{2} = U_1(B,D)^2 + U_2(B,D,M,\alpha,t)^2 + U_3(B,D,M)^2 + U_4(B,D,M,SF,t,\mathrm{scene})^2 + U_5(B,D,M,SF,t,\mathrm{scene})^2. \tag{14}$$

The first term, U_1, contains the terms of the SD calibration uncertainty, which are considered to be constant in time, including the earthshine impact. The second term, U_2, represents the RVS uncertainty as well as uncertainty in the m_1 not accounted for in U_1. The U_2 term is both time- and AOI-dependent and varies depending on the band and whether the on-board RVS algorithm or the EV-based RVS algorithm is used. The third term, U_3, represents the uncertainty in the instrument temperature correction, which is based on prelaunch measurements and is band, detector, and mirror-side dependent. The fourth term, U_4, contains the scene-dependent uncertainty in dn_{EV} and is derived from the SD calibration measurements. The final term, U_5, is an additional term, not derived from the above equations, that accounts for uncertainty due to optical leak and electronic crosstalk in the SWIR bands. It is assigned to be equal to one-fourth of the SWIR dn_{EV} correction ($\Delta dn_{\mathrm{EV}}/dn_{\mathrm{EV}}$). At typical radiance levels for both sending and receiving bands, this term (averaged over operable detectors and sub-frames) could be from 0.2% to 2.0% for Terra MODIS SWIR bands with the largest uncertainty for band 5. With less optical leak and electronic crosstalk, the Aqua SWIR band uncertainty is smaller than for Terra MODIS.

The total uncertainty for the Terra and Aqua MODIS RSB is shown for multiple years in Fig. 3. The results shown are for mirror side 1 and averaged over all operable detectors (i.e., excluding noisy and inoperable). The contributions from the uncertainty due to optical leak and electronic crosstalk in the SWIR bands (U_5 term) are not included in the results in this figure. This term is scene dependent and can add significantly to the displayed uncertainty of the SWIR bands for low radiance scenes. As seen for the nadir case in Fig. 3, most Terra MODIS RSB continue to meet the 2% specification after multiple years on-orbit. The bands that use EV-based calibration (1 to 4 and 8 to 10) have relatively high uncertainty compared with the other RSB due to the larger variances in the retrieved EV data compared with the SD and lunar data. It is also observed that bands 5, 7, and 18 marginally exceed the 2% specification. In comparison with other RSB, the typical radiance values for these bands (see Table 1) are relatively low. This translates to a lower SNR and a larger uncertainty (U_4 term).

Differences in uncertainty across different scan angles (nadir, −45 deg and +45 deg) are due entirely to the uncertainty in RVS, which is contained in the U_2 term. As discussed earlier, the bands that use EV-based calibration tend to have larger uncertainty, and this is particularly true for the short-wavelength VIS bands (3, 8, 9, and 10). In addition, on-orbit polarization sensitivity of the Terra MODIS SM is known to have changed especially for these short wavelength bands 8 and 9 at the end of scan (high scan angles), and this is likely the reason that the uncertainties for these bands are much larger at higher scan angles. In general, the uncertainty at the SV scan angle (close to the case at scan angle of −45 deg) calculated using lunar measurements has much smaller magnitude than other angles that rely on the EV desert targets. In the case of bands 1 and 2, the EV data are used at all the scan angles due to disagreement between the on-orbit lunar and EV measurements; hence the uncertainty at all angles is between 1.8% and 2.4%. In general, the uncertainty results observed in Aqua MODIS RSB are very similar in trend, but of a slightly lower magnitude, in comparison with Terra MODIS. Unlike Terra MODIS, the on-orbit change in the polarization sensitivity of Aqua MODIS is known to be minimal, which is reflected in the results at +45 deg scan angle for the short wavelength bands 8 and 9.

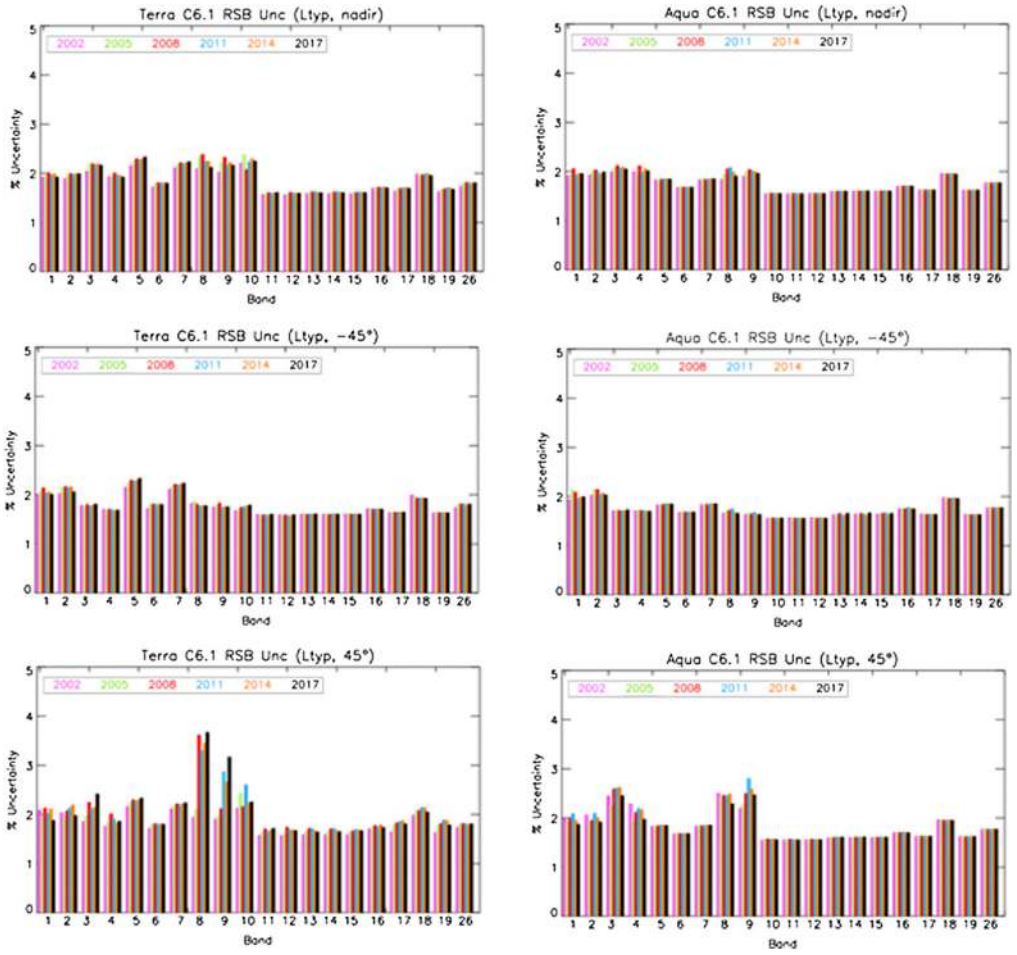

Fig. 3 Terra and Aqua MODIS RSB uncertainty at typical radiance and three scan-angles (nadir, −45 deg and +45 deg).

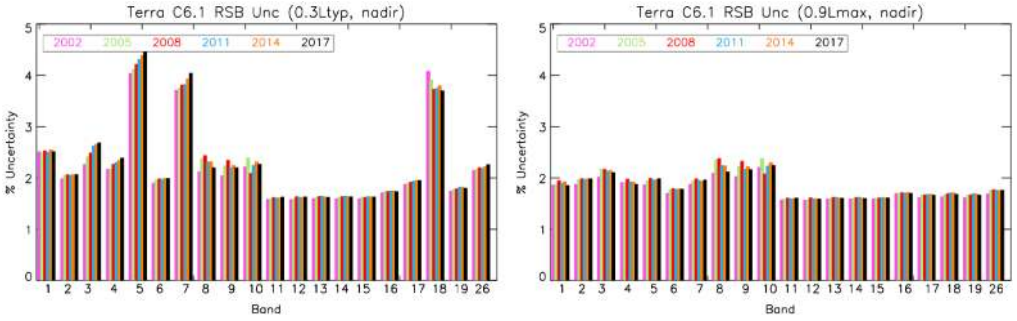

Fig. 4 Terra MODIS RSB uncertainty (nadir) at specified 0.3 typical radiance and 0.9 maximum radiance levels.

Figure 4 shows the uncertainty of the Terra MODIS RSB (nadir) at two ends of the dynamic range, i.e., $0.3L_{\text{typical}}$ and $0.9L_{\text{max}}$. As discussed earlier, the scene-dependent term U_4 increases at lower scene radiances, resulting in greater uncertainties for all RSB. It should be noted that the specified uncertainty requirement of 2% in reflectance for the RSB is for observations at typical scene radiance level. An extra 1% uncertainty is added to specified requirements for observations made at different radiance levels from 0.3 L_{typ} to 0.9 L_{max}. With this criterion, only bands 5, 7, and 18 are seen to exceed the specification for reasons discussed earlier. Similar results for Aqua MODIS are shown in Fig. 5.

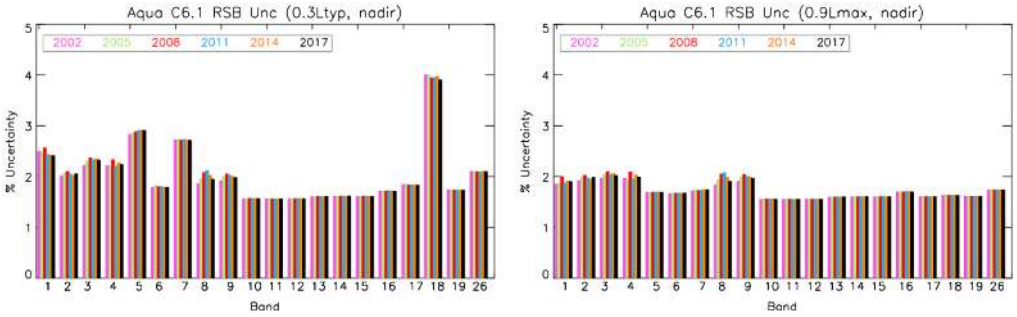

Fig. 5 Aqua MODIS RSB uncertainty (nadir) at specified 0.3 typical radiance and 0.9 maximum radiance levels.

4 Thermal Emissive Bands Calibration Uncertainty

From TEB calibration Eqs. (7) and (8), the EV radiance can be expressed as

$$L_{\mathrm{EV}} = \frac{1}{\mathrm{RVS}_{\mathrm{EV}}}\left\{(a_0 + a_2 \cdot dn_{\mathrm{EV}}^2) + [\mathrm{RVS}_{\mathrm{BB}} \cdot \varepsilon_{\mathrm{BB}} \cdot L_{\mathrm{BB}} + (\mathrm{RVS}_{\mathrm{SV}} - \mathrm{RVS}_{\mathrm{BB}}) \cdot L_{\mathrm{SM}} + \mathrm{RVS}_{\mathrm{BB}} \cdot (1 - \varepsilon_{\mathrm{BB}}) \cdot \varepsilon_{\mathrm{CAV}} \cdot L_{\mathrm{CAV}} - a_0 - a_2 \cdot dn_{\mathrm{BB}}^2] \cdot \frac{dn_{\mathrm{EV}}}{dn_{\mathrm{BB}}} - (\mathrm{RVS}_{\mathrm{SV}} - \mathrm{RVS}_{\mathrm{EV}}) \cdot L_{\mathrm{SM}}\right\}. \tag{15}$$

It is a function of several parameters determined from prelaunch and on-orbit observations

$$L_{\mathrm{EV}} = L_{\mathrm{EV}}\{a_0, a_2, \mathrm{RVS}_{\mathrm{BB}}, \mathrm{RVS}_{\mathrm{SV}}, \mathrm{RVS}_{\mathrm{EV}}, \varepsilon_{\mathrm{BB}}, \varepsilon_{\mathrm{CAV}}, \lambda, T_{\mathrm{BB}}, T_{\mathrm{SM}}, T_{\mathrm{CAV}}, dn_{\mathrm{EV}}, dn_{\mathrm{BB}}\}. \tag{16}$$

The TEB calibration uncertainty is determined by combining the contributions from all of the parameters involved in the calibration and retrieval. In our analysis, the contributions from higher order and cross-product terms are not considered as they are either much smaller than the first-order terms or uncorrelated. With these assumptions, the total uncertainty of L_{EV} can be computed using a small perturbation approach

$$\left(\frac{dL_{\mathrm{EV}}}{L_{\mathrm{EV}}}\right)^2 = \sum_i \left[\frac{L_{\mathrm{EV}}(x_i + dx_i) - L_{\mathrm{EV}}(x_i)}{L_{\mathrm{EV}}(x_i)}\right]^2, \tag{17}$$

where x_i represents a given contributing parameter in Eq. (16) and dx_i represents the measurement error or estimated uncertainty for parameter x_i. Tables 3 and 4 provide examples of Terra and Aqua MODIS TEB calibration uncertainties implemented in the C6 L1B with contributions from individual parameters. The uncertainties (for year 2008) are expressed as a percentage of the typical radiance level and at nadir AOI. With the exception of Terra LWIR PV bands (27 to 30), the uncertainties listed in Tables 3 and 4 are nearly identical to that used for C6.1 L1B.

The Terra MODIS PC bands, 32 to 36, have an additional uncertainty imposed due to signal contamination from an optical leak (PCX). This is not the case for Aqua MODIS. As expected, the Terra MODIS TEB uncertainty for these five bands is generally higher than Aqua MODIS. MODIS band 21 (for fire detection), with a calibration uncertainty requirement of 10%, has been calibrated in the L1B using a fixed linear coefficient. Its calibration uncertainties shown in Tables 3 and 4 are not adequate and need to be determined separately.

Although the same uncertainty values of the BB (50 mK), SM (1.0 K), and CAV (1.0 K), temperatures are used for all TEB, their impacts on the calibration uncertainties are spectral band and retrieval radiance-level dependent. The center wavelength (CW) uncertainty was determined from prelaunch spectral characterization.[32] The BB spectral emissivity and its uncertainty were characterized prelaunch using thermal vacuum calibration datasets.[33,34] Meanwhile, the scan cavity emissivity and its uncertainty values were estimated based on the instrument design and characteristics. The impact of this term on the total calibration uncertainty is usually very

Table 3 Terra MODIS TEB calibration uncertainties (at typical radiance, nadir AOI, year 2008, C6).

Band	T_BB	T_SM	T_CAV	CW	RVS_EV	RVS_SV	ε_BB	ε_CAV	dn_BB	dn_EV	a_0	a_2	PCX	RSS (%)
20	0.23	0.00	0.01	0.43	0.08	0.02	0.11	0.02	0.02	0.11	0.00	0.02	0.00	0.52
21	0.00	0.00	0.00	0.00	2.19	0.26	0.00	0.00	0.00	0.49	0.00	0.00	0.00	2.34
22	0.22	0.00	0.01	0.38	0.08	0.02	0.11	0.02	0.02	0.11	0.00	0.03	0.00	0.47
23	0.21	0.00	0.02	0.36	0.07	0.02	0.16	0.02	0.02	0.09	0.00	0.03	0.00	0.47
24	0.18	0.01	0.02	0.26	0.23	0.27	0.19	0.03	0.01	0.67	0.04	0.05	0.00	0.84
25	0.19	0.00	0.02	0.26	0.01	0.05	0.15	0.03	0.02	0.22	0.01	0.02	0.00	0.42
27	0.13	0.03	0.02	0.14	0.19	0.22	0.12	0.03	0.01	0.50	0.23	0.07	0.00	0.67
28	0.11	0.02	0.02	0.09	0.05	0.07	0.16	0.04	0.01	0.18	0.05	0.22	0.00	0.37
29	0.10	0.03	0.02	0.04	0.03	0.01	0.11	0.05	0.01	0.05	0.01	0.10	0.00	0.21
30	0.09	0.06	0.01	0.01	0.10	0.15	0.14	0.04	0.02	0.25	0.09	0.42	0.00	0.56
31	0.08	0.01	0.01	0.02	0.02	0.01	0.06	0.03	0.01	0.04	0.00	0.03	0.00	0.12
32	0.07	0.01	0.01	0.03	0.02	0.01	0.03	0.02	0.01	0.05	0.00	0.03	0.00	0.11
33	0.07	0.03	0.01	0.04	0.04	0.06	0.03	0.03	0.02	0.22	0.00	0.06	0.11	0.28
34	0.07	0.04	0.01	0.04	0.31	0.33	0.06	0.03	0.03	0.32	0.00	0.11	0.16	0.60
35	0.07	0.05	0.01	0.04	0.16	0.18	0.03	0.03	0.03	0.46	0.00	0.09	0.22	0.59
36	0.07	0.07	0.01	0.04	0.40	0.42	0.06	0.03	0.05	1.01	0.00	0.10	0.52	1.28

small. For a given spectral band, several contributors in Eq. (17) are constant and in general their impact on the total uncertainty is relatively small. The a_0, a_2, dn_{EV}, and dn_{BB} terms are time dependent and can have large impact on the total uncertainty, depending on the detector performance and calibration quality. It should also be noted that some TEB on-orbit calibrations are made with the a_0 terms set to zero. Table 5 shows the TEB calibration uncertainty at different radiance levels. Except for a few bands in Terra MODIS at lower radiance levels, most TEB continue to meet the calibration requirements.

The uncertainty values for Terra MODIS bands 27 to 30 (Tables 3 and 5) are inadequately estimated as no correction for electronic crosstalk was included in C_6. The latest L1B (C6.1) calibration algorithm has included an electronic crosstalk correction for these bands. As shown in Fig. 6 are examples of Terra and Aqua MODIS TEB on-orbit calibration uncertainties in C6.1 for select years at their typical radiances and three scan-angles (nadir, -45 deg and $+45$ deg). The updated results indicate a significant reduction of uncertainty, particularly in Terra bands 27 and 30 after 2015, which is due to improvement of the stability in a_0/a_2 and detector noise after the crosstalk correction. Figures 7 and 8 show the uncertainties at 0.3 of typical and 0.9 of maximum radiances for Terra and Aqua MODIS, respectively. As expected, at the 0.3 typical radiance there is a significant increase in uncertainty for bands with low typical temperatures.

To account for the electronic crosstalk correction in the calculation of the L1B radiance uncertainty, we apply an additional penalty term at the pixel level for each detector (i) in these bands, as given by

$$P_i = \frac{\Delta dn}{dn}\beta_i, \tag{18}$$

where Δdn is the magnitude of the signal correction, dn is the corrected signal level, and β_i is the uncertainty penalty coefficient for a given detector. The appropriate value for β_i is found by

Table 4 Aqua MODIS TEB calibration uncertainties (at typical radiance, nadir AOI, year 2008, C6).

Band	t_bb	t_sm	t_cav	CW	rvs_ev	rvs_sv	ε_BB	s_CAV	dn_BB	dn_EV	a_0	a_2	PCX	RSS (%)
20	0.23	0.00	0.00	0.44	0.01	0.01	0.26	0.00	0.03	0.10	0.09	0.03	0.00	0.58
21	0.00	0.00	0.00	0.00	0.08	0.02	0.00	0.00	0.00	0.64	0.00	0.00	0.00	0.64
22	0.22	0.00	0.00	0.39	0.02	0.01	0.25	0.00	0.02	0.08	0.08	0.08	0.00	0.54
23	0.22	0.00	0.00	0.37	0.01	0.01	0.25	0.00	0.02	0.08	0.09	0.09	0.00	0.52
24	0.19	0.03	0.00	0.27	0.04	0.05	0.19	0.00	0.02	0.60	0.30	0.09	0.00	0.78
25	0.20	0.01	0.00	0.27	0.00	0.01	0.19	0.00	0.02	0.17	0.06	0.06	0.00	0.43
27	0.13	0.03	0.00	0.14	0.21	0.24	0.15	0.00	0.01	0.35	0.21	0.09	0.00	0.58
28	0.12	0.02	0.00	0.10	0.03	0.03	0.15	0.01	0.01	0.13	0.15	0.11	0.00	0.32
29	0.10	0.01	0.01	0.04	0.04	0.02	0.14	0.02	0.01	0.03	0.03	0.07	0.00	0.20
30	0.09	0.03	0.01	0.01	0.08	0.07	0.13	0.04	0.01	0.17	0.17	0.15	0.00	0.35
31	0.08	0.01	0.00	0.01	0.00	0.00	0.12	0.00	0.00	0.02	0.00	0.04	0.00	0.16
32	0.07	0.01	0.00	0.02	0.00	0.00	0.12	0.01	0.01	0.04	0.00	0.02	0.00	0.15
33	0.08	0.03	0.00	0.04	0.00	0.01	0.10	0.00	0.02	0.17	0.03	0.05	0.00	0.23
34	0.07	0.04	0.00	0.04	0.01	0.01	0.09	0.00	0.02	0.20	0.07	0.09	0.00	0.26
35	0.08	0.05	0.00	0.04	0.02	0.02	0.10	0.01	0.03	0.30	0.05	0.08	0.00	0.34
36	0.07	0.08	0.00	0.04	0.05	0.03	0.12	0.01	0.03	0.52	0.21	0.21	0.00	0.63

comparing the long-term drift in the band-averaged, corrected radiance to a relatively stable reference, in this case band 31, over warm ocean scenes where the radiance is relatively high. For bands 27 to 30, the drift in corrected radiance relative to band 31 is on the order of 1% over the course of the mission. We then choose a value β_i such that the band-averaged value of the applied penalty is equal to that of the measured radiance drift after correction for selected scenes late in the mission.

For bands 28 to 30, we calculated β_i to be 0.040, 0.095, and 0.021, respectively. The same values are applied to each detector within the band. For band 27, $\beta_i = 0.025$ for detectors 3to 8 and 0.0375 for detectors 1, 2, 9, and 10 due to the higher levels of contamination for these detectors relative to the rest of the band. As the applied penalty is proportional to the magnitude of the corrected signal, the uncertainty penalty is dependent on the detector, scene, and time during the mission, with the assessed penalty generally increasing as the mission progresses. For high-radiance scenes late in the mission, most detectors are generally assessed an uncertainty penalty of 1% to 2%, with some detectors in band 27 having a 3% to 5% penalty. Early in the mission, the uncertainty penalty is negligible for all detectors.

5 Future Improvements

In addition to changes with on-orbit calibration algorithms, several enhancements can be made to improve the assessments of MODIS calibration uncertainties. The MODIS SD panel's BRF was characterized prelaunch by the instrument vendor using reference samples traceable to NIST reflectance standards at a number of wavelengths up to 1.7 μm. No direct BRF measurements were made at 2.1 μm due to low SNR and hence an extrapolation is used, contributing an additional 0.5% uncertainty at 2.1 μm (band 7) that is not accounted for in our current SD BRF

Table 5 Summary of Terra and Aqua MODIS TEB calibration uncertainty (C6) in percentage at different radiance levels (nadir view, year 2008, C6).

	Terra			Aqua		
Bands	L_{typ}	0.3 L_{typ}	0.9 L_{max}	L_{typ}	0.3 L_{typ}	0.9 L_{max}
20	0.52	0.61	0.56	0.58	0.68	0.63
22	0.47	0.57	0.51	0.54	0.60	0.63
23	0.47	0.55	0.50	0.52	0.58	0.65
24	0.84	2.73	0.56	0.78	2.36	0.54
25	0.42	0.92	0.40	0.43	0.85	0.41
27	0.67	2.34	0.34	0.58	1.88	0.30
28	0.37	0.88	0.26	0.32	0.91	0.24
29	0.21	0.45	0.33	0.20	0.32	0.25
30	0.56	1.47	0.31	0.35	1.25	0.22
31	0.12	0.25	0.14	0.16	0.23	0.19
32	0.11	0.27	0.13	0.15	0.22	0.17
33	0.28	0.98	0.22	0.23	0.58	0.19
34	0.60	3.29	0.43	0.26	0.88	0.22
35	0.59	2.08	0.46	0.34	0.94	0.29
36	1.28	4.31	1.02	0.63	2.01	0.50

uncertainty estimate (Table 2). Also considered are the improvements of SWIR on-orbit calibration for both Terra and Aqua MODIS by applying correction for the SD degradation, and the use of a different sending band for Terra MODIS SWIR optical leak and electronic crosstalk correction as several detectors in the current sending band (B28) have also been significantly impacted by the electronic crosstalk from the other LWIR PV bands.[35] Other improvements are listed in the following for future considerations

- RSB mirror side 2 uncertainty for bands using mirror side 1 as reference

  As discussed in Sec. 3, some of the bands that use the on-board based RVS calibration use additional mirror side ratio data from EV ocean targets to correct the RVS of mirror side 2 relative to mirror side 1. This is currently applied to Aqua bands 10 to 16 and Terra bands 11 to 16. As a result, an additional uncertainty term is included only for mirror side 2, which is not desirable. One option for resolving this is to change the RVS calibration such that the EV mirror-side ratio correction is applied equally to the RVS of both mirror sides (while maintaining the ratio). Then, the additional uncertainty term should also be applied equally to both mirror sides.

- RSB RVS uncertainty for bands that have been impacted by the changes in sensor polarization sensitivity

  Current RSB calibration coefficients are derived under the assumption that the impact due to instrument polarization sensitivity is small and can be ignored. Several Terra MODIS VIS spectral bands (e.g., bands 8 and 9), however, have seen large changes (increases) in their polarization sensitivity, especially at the large AOIs.[36] Because of this, the RVS derived using EV targets at different AOIs is affected due to an increase in the instrument polarization sensitivity. As a potential improvement, the EV based RVS should be derived after removing the polarization effect.

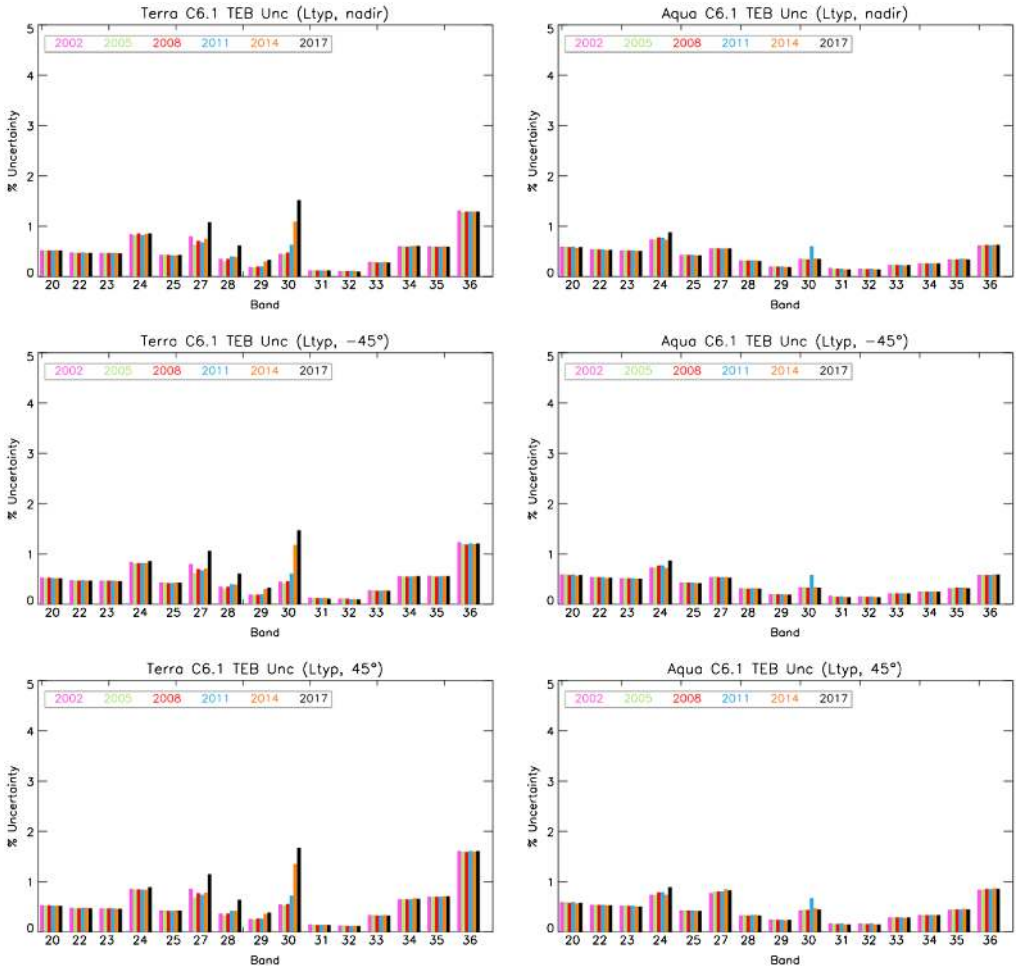

Fig. 6 Terra and Aqua MODIS TEB uncertainty (C6.1) at typical radiance and three scan-angles (nadir, −45 deg and +45 deg).

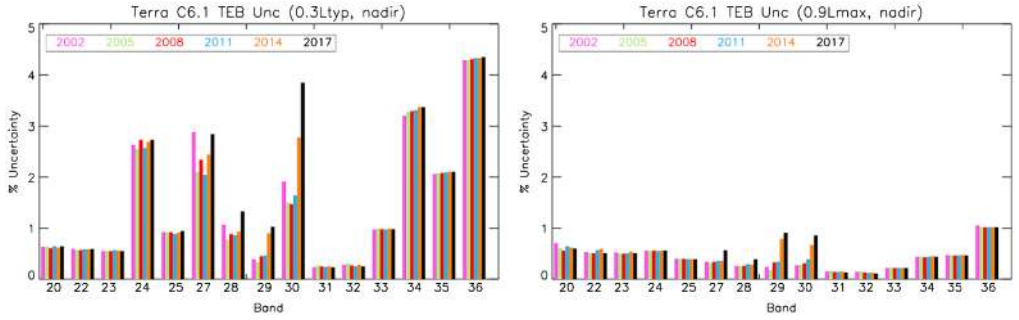

Fig. 7 Terra MODIS TEB uncertainty (C6.1, nadir) at specified 0.3 typical radiance and 0.9 maximum radiance levels.

- TEB uncertainty for bands using fixed calibration coefficients during BB warm-up and cool-down (WUCD)

  Fixed gain coefficients, i.e., default b_1, are used for Aqua bands 33, 35, and 36 during BB warm-up and cool-down when the detector responses saturate over certain high BB temperatures. During this period, the default b_1 values are predetermined using BB measurements from three consecutive orbits generally 10 days before each BB WUCD. As these values are not computed from instantaneous scan–by–scan measurements, an extra, small uncertainty term needs to be considered when the default b_1 is used.

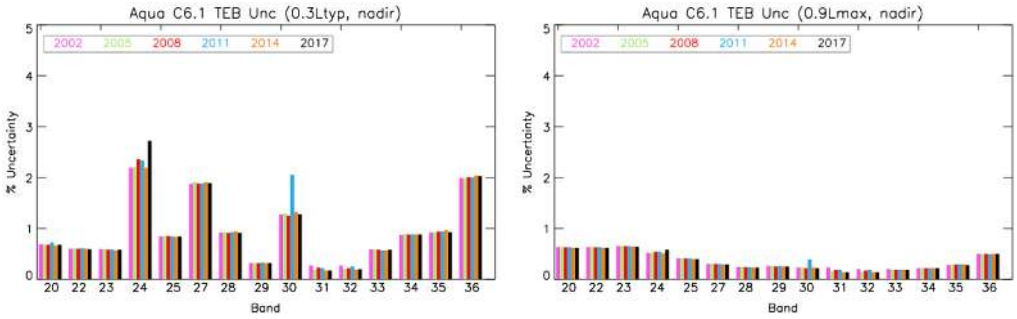

Fig. 8 Aqua MODIS TEB uncertainty (C6.1, nadir) at specified 0.3 typical radiance and 0.9 maximum radiance levels.

- B21 calibration uncertainty

  Unlike most TEB, band 21 uses a simple linear calibration algorithm. Its b_1 coefficients are provided via an LUT with its values derived from BB WUCD. As this low-gain band is primarily used for fire detection with a specified maximum temperature of 500 K, its response to the BB nominal temperature (290 K for Terra and 285 for Aqua) is at the low end of its dynamic range. Because of this, the calibration uncertainty could be very large when scene temperatures are considerably high (e.g., for fire scene).

- TEB RVS uncertainty for Terra MODIS using new deep space maneuver data sets

  Terra MODIS TEB RVS used in the current L1B product is based on the results derived from a deep space maneuver performed in 2003. In August 2017, Terra conducted another deep space maneuver. A comparison of the TEB RVS derived from these two maneuvers shows that the differences are generally within 0.2% except for the bands 27 to 30 that in recent years have large electronic crosstalk. The differences are small but comparable with the RVS uncertainties currently assigned for most TEB. As a future improvement, a better estimate of the TEB RVS can be made by combing the RVS results from both maneuvers and relative long-term trends (time series) using other stable targets.

6 Summary

The MODIS instruments have been successfully operating on-orbit making continuous global observations for various science applications. In comparison with its predecessors, MODIS has a more stringent requirement on its calibration accuracy and data product quality. A sustained instrument characterization program has led to timely upgrades to the L1B algorithm, resulting in well calibrated science products that continue to meet the overall science requirements. Algorithms used to estimate the calibration uncertainties on-orbit for both the RSB and TEB are discussed in detail. This paper serves as an update to our previous uncertainty analysis results reflecting the calibration algorithm updates performed over the mission of each instrument. With a few exceptions, most RSB and TEB calibration uncertainties are within the specified uncertainty requirements. Due to the significant on-orbit degradation observed in the short wavelength bands, the OBC measurements are supplemented with EV data from time-invariant desert sites. The changing polarization sensitivity of short wavelength Terra MODIS bands (3, 8, 9, and 10) at large AOIs has contributed to the increased uncertainty as the RVS for these bands, which is derived from the EV measurements. With the addition of the electronic crosstalk correction for bands 27 to 30 in Terra MODIS C6.1, our assessment of the uncertainty in these bands also needed to be re-evaluated. With the algorithm change and correction applied in C6.1, the uncertainty for these bands was reduced significantly during the more recent years of the mission. Several enhancements to the current approach were also identified and will be considered for a future L1B version.

Acknowledgments

The authors would like to thank all current and past members of MCST for their many and varied contributions over the years. They would also like to thank the Science Team members they have collaborated with, leading to greater understanding of instrument performance, impacts on the science products, and improvements in their calibration methodologies. This manuscript is an extension of an SPIE conference proceedings paper, Xiong, X., A. Angal, W. Barnes, H. Chen, V. Chiang, X. Geng, Y. Li, K. Twedt, Z. Wang, T. Wilson, et al., "Updates of MODIS on-orbit calibration uncertainty assessments," Proc. SPIE—Earth Observing Systems XXII, vol. 10402, no. 104020M, 2017.

References

1. W. L. Barnes and V. V. Salomonson, "MODIS: a global image spectroradiometer for the earth observing system," *Crit. Rev. Opt. Sci. Technol.* **47**, 285–307 (1993).
2. W. L. Barnes et al., "Development, characterization, and performance of the EOS MODIS sensors," *Proc. SPIE* **5151**, 337–345 (2003).
3. X. Xiong et al., "NASA EOS terra and aqua MODIS on-orbit performance," *Adv. Space Res.* **43**, 413–422 (2008).
4. X. Xiong, B. N. Wenny, and W. L. Barnes, "Overview of NASA earth observing systems terra and aqua moderate resolution imaging spectroradiometer instrument calibration algorithms and on-orbit performance," *J. Appl. Remote Sens.* **3**, 032501 (2009).
5. C. Schueler et al., "NPOESS VIIRS sensor design overview," *Proc. SPIE* **4483**, 11–23 (2001).
6. R. P. Murphy et al., "The visible infrared imaging radiometer suite," in *Earth Science Satellite Remote Sensing*, J. J. Qu et al., Eds., Vol. **1**, pp. 199–223, Springer-Verlag, Berlin, Heidelberg (2006).
7. E. J. Knight and G. Kvaran, "Landsat-8 operational land imager design, characterization and performance," *Remote Sens.* **6**, 10286–10305 (2014).
8. B. Markham, "Landsat-8 operational land imager radiometric calibration and stability," *Remote Sens.* **6**, 12275–12308 (2014).
9. V. V. Salomonson, "An overview of the earth observing system MODIS instrument and associated data systems performance," in *IEEE Int. Geoscience and Remote Sensing Symp.*, Vol. 2, pp. 1174–1176 (2002).
10. V. Salomonson and X. Xiong, "MODIS instrument characteristics, performance, and data for climate studies," in *Satellite-Based Applications on Climate Change*, J. Qu, A. Powell, and M. Sivakumar, Eds., pp. 31–48, Springer, Dordrecht (2013).
11. X. Xiong, A. Isaacman, and W. L. Barnes, "MODIS level-1B products," in *Earth Science Satellite Remote Sensing: Science and Instrument*, J. J. Qu et al., Eds., Vol. **1**, pp. 33–49, Springer, Berlin, Heidelberg (2006).
12. G. Toller, "Status of EOS terra and aqua MODIS L1B algorithm," *J. Appl. Remote Sens.* **2**, 023505 (2008).
13. G. Toller et al., "Terra and aqua moderate-resolution imaging spectroradiometer collection 6 level 1B algorithm," *J. Appl. Remote Sens.* **7**, 073557 (2013).
14. GSFC, "Specification for the moderate resolution imaging spectroradiometer," GSFC 422-20-02, Rev. A, Goddard Space Flight Center (1993).
15. J. Esposito, "MODIS reflective solar bands uncertainty analysis," *Proc. SPIE* **5542**, 448–458 (2004).
16. K. Chiang et al., "MODIS thermal emissive bands calibration uncertainty analysis," *Proc. SPIE* **5542**, 437–447 (2004).
17. X. Xiong et al., "Terra and aqua MODIS calibration algorithms and uncertainty analysis," *Proc. SPIE* **5978**, 59780V (2005).
18. K. Chiang, J. McIntire, and X. Xiong, "VIIRS thermal emissive bands L1B calibration uncertainty," in *IEEE Int. Geoscience and Remote Sensing Symp. (IGARSS)*, pp. 4197–4200 (2017).
19. N. Lei et al., "SNPP VIIRS RSB Earth view reflectance uncertainty," in *IEEE Int. Geoscience and Remote Sensing Symp. (IGARSS)*, pp. 5916–5919 (2017).

20. X. Xiong and J. Butler, "MODIS solar reflective calibration traceability," *Proc. SPIE* **7452**, 74520K (2009).
21. X. Xiong et al., "Multi-year on-orbit calibration and performance of terra MODIS reflective solar bands," *IEEE Trans. Geosci. Remote Sens.* **45**(4), 879–889 (2007).
22. X. Xiong et al., "Multiyear on-orbit calibration and performance of terra MODIS thermal emissive bands," *IEEE Trans. Geosci. Remote Sens.* **46**(6), 1790–1803 (2008).
23. X. Xiong et al., "Aqua MODIS thermal emissive bands on-orbit calibration, characterization, and performance," *IEEE Trans. Geosci. Remote Sens.* **47**(3), 803–814 (2009).
24. X. Xiong et al., "On-orbit calibration and performance of aqua MODIS reflective solar bands," *IEEE Trans. Geosci. Remote Sens.* **48**(1), 535–546 (2010).
25. X. Xiong et al., "MODIS correction algorithm for out-of-band response in the short-wave IR bands," *Proc. SPIE* **5234**, 605–613 (2004).
26. T. Wilson et al., "Development and implementation of an electronic crosstalk correction for bands 27-30 in terra MODIS collection 6," *Remote Sens.* **9**(6), 569 (2017).
27. M. Pavlov, M. Byers, and J. A. Walker, "Bidirectional reflectance factor (BRF) characterization of the MODIS flight solar diffuser, earth observing systems III," *Proc. SPIE* **3439**, 257–268 (1998).
28. X. Xiong et al., "On-orbit characterization of a solar diffuser's bidirectional reflectance factor using spacecraft maneuvers, earth observing systems VIII," *Proc. SPIE* **5151**, 375–383 (2003).
29. A. Angal et al., "On-orbit noise characterization of MODIS reflective solar bands," *J. Appl. Remote Sens.* **9**, 094092 (2015).
30. J. Sun et al., "Time-dependent response versus scan angle for MODIS reflective solar bands," *IEEE Trans. Geosci. Remote Sens.* **52**(6), 3159–3174 (2014).
31. A. Angal et al., "On-orbit performance and calibration improvements for the reflective solar bands of terra and aqua MODIS," *Proc. SPIE* **9881**, 98811F (2016).
32. J. B. Young, "MODIS calibration and accuracy areas," Internal Rep. SBRS (1997).
33. X. Wang et al., "MODIS OBC emissivity extracted from RC02 and MFI09 data sets," MCST Internal Memorandum (1999).
34. A. Wu and X. Xiong, "Re-evaluation of MODIS OBC BB emissivity uncertainty," MCST Internal Memorandum (2005).
35. K. Twedt et al., "MODIS solar diffuser degradation at short-wave infrared band wavelengths," *Proc. SPIE* **10402**, 104022K (2017).
36. A. Wu et al., "Assessment of terra MODIS on-orbit polarization sensitivity using pseudo-invariant desert sites," *IEEE Trans. Geosci. Remote Sens.* **55**(7), 4168–4176 (2017).

Xiaoxiong Xiong is an optical physicist at NASA/GSFC, currently serving as the MODIS Project Scientist and the MODIS and VIIRS Calibration Scientist. He received his BS degree in optical engineering from Beijing Institute of Technology, Beijing, China and his PhD in physics from University of Maryland, College Park, Maryland, USA. In addition to remote sensing, he had also worked in the fields of optical instrumentation, nonlinear optics, laser/atomic spectroscopy, and mass spectrometry, http://science.gsfc.nasa.gov/sed/bio/xiaoxiong.xiong-1.

Biographies for the other authors are not available.